WOODS HOLE OCEANOGRAPHIC INSTITUTION
1930
Deep Submergence Laboratory

13 August 1998

Dr. Thomas B. Curtin, ONR 322
Office of Naval Research
Ballston Tower One
800 North Quincy Street
Arlington, VA 22217-5660

Dear Dr. Curtin:

Enclosed is the final report for ONR grant N00014-96-1-5014, entitled "A Practical Hydrodynamic-Based Model of AUV Thruster Dynamics for Use in Closed-Loop Control of Vehicle Motions," Principal Investigator: Mark A. Grosenbaugh.

Sincerely,

Larry D. Flick
DSL Center Administrator

cc: D. Rideout, Administrative Contracting Officer
Director, Naval Research Laboratory
Defense Technical Information Center
M. Tavares, Grant and Contract Services
AOPE Department Office
DSL files

REPORT DOCUMENTATION PAGE

Form Approved
OMB No. 0704-0188

1. AGENCY USE ONLY *(Leave blank)*	2. REPORT DATE	3. REPORT TYPE AND DATES COVERED

4. TITLE AND SUBTITLE

A Practical Hydrodynamic-Based Model of AUV Thruster Dynamics for Use in Closed-Loop control of Vehicle Motions.

5. FUNDING NUMBERS

N000-14-96-1-5014

6. AUTHOR(S)

Mark A. Grosenbaugh and Louis L. Whitcomb

7. PERFORMING ORGANIZATION NAMES(S) AND ADDRESS(ES)

Woods Hole Oceanographic Instituition
Applied Ocean Physic and Engineering Department
Woods Hole, MA. 02543

8. PERFORMING ORGANIZATION REPORT NUMBER

9. SPONSORING / MONITORING AGENCY NAMES(S) AND ADDRESS(ES)

10. SPONSORING / MONITORING AGENCY REPORT NUMBER

11. SUPPLEMENTARY NOTES

a. DISTRIBUTION / AVAILABILITY STATEMENT

Approved for public reslease, distribution is unlimited

12. DISTRIBUTION CODE

13. ABSTRACT ***(Maximum 200 words)***

This report documents two novel improvements in the finite-dimensional nonlinear dynamical modeling of marine thrusters. Previously reported models, which fail to capture many of the characteristic nonlinear reponses that occur during unsteady operations, assume that the lift and drag forces on the propeller blades are proportional to the sine and cosine of the angle of attack where the angle of attack is a function of the axial flow velocity and the propeller's angular velocity. We have found that the lift and drag forces are not sinusoidal. We have also incorporated the effects of rotational fluid velocity and inertia on thruster response. The force curves and model parameters are identified using experimental data from the load cell and acoustic doppler current meters. The accuracy of the model is determined by comparing experimental performance with numerical simulations. The results indicate that thruster models with nonsinusoidal lif and drag curves provide superior accuracy in both transient and steady-state response. Incorporating rotational fluid velocities into our model gave an insignificant improvement for our case. However, rotational fluid flow may be important for other types of thrusters. The research performed under this grant was reported in [9, 4, 14, 3, 5] and is referenced at the end of the text.

14. SUBJECT TERMS

Thruster Dynamics, Closed-Loop control

15. NUMBER OF PAGES

16. PRICE CODE

17. SECURITY CLASSIFICATION OF REPORT	18. SECURITY CLASSIFICATION OF THIS PAGE	19. SECURITY CLASSIFICATION OF ABSTRACT	20. LIMITATION OF ABSTRACT
unclassified	unclassified	unclassified	unclassified

A Practical Hydrodynamic-Based Model of AUV Thruster Dynamics for Use in Closed-Loop Control of Vehicle Motions

Final Report for Grant Number N00014-96-1-5014

MARK A. GROSENBAUGH & LOUIS L. WHITCOMB *

Abstract

This report documents two novel improvements in the finite-dimensional nonlinear dynamical modeling of marine thrusters. Previously reported models, which fail to capture many of the characteristic nonlinear reponses that occur during unsteady operations, assume that the lift and drag forces on the propeller blades are proportional to the sine and cosine of the angle of attack where the angle of attack is a function of the axial flow velocity and the propeller's angular velocity.

We have found that the lift and drag forces are not sinusoidal. We have also incorporated the effects of rotational fluid velocity and inertia on thruster response. The force curves and model parameters are identified using experimental data from the load cell and acoustic doppler current meters. The accuracy of the model is determined by comparing experimental performance with numerical simulations. The results indicate that thruster models with nonsinusoidal lift and drag curves provide superior accuracy in both transient and steady-state response. Incorporating rotational fluid velocities into our model gave an insignificant improvement for our case. However, rotational fluid flow may be important for other types of thrusters. The research performed under this grant was reported in [9, 4, 14, 3, 5] and is referenced at the end of the text.

1 Introduction

Recent advances in underwater position and velocity sensing enable real-time *cm*-precision position measurements of underwater vehicles [19, 6, 11, 7, 2, 17]. With these advances in position sensing, our ability to precisely control the hovering and low-speed trajectory of an underwater vehicle is limited principally by our understanding of (*i*) the vehicle's dynamics and (*ii*) the dynamics of the bladed thrusters commonly used to actuate dynamically-positioned marine vehicles. This paper addresses the latter problem. Recent results indicate that the transient (unsteady) dynamics of marine thrusters can be approximated by a simple nonlinear finite-dimensional lumped-parameter dynamical system [18, 1, 12, 8, 16]. In [8] the authors report a nonlinear thruster dynamics model based on the motor electro-mechanical dynamics and thin-foil propeller hydrodynamics. In this model, the propeller and fluid dynamics are approximated by a two-dimensional second order nonlinear dynamical system with state variables of (*i*) axial fluid velocity and (*ii*) propeller rotational velocity. We will refer to this model as the "axial flow model". In [16] the authors report experiments that corroborate the utility of the axial flow model, but also identify discrepancies between experimental thruster transient response and that predicted by the model.

This paper is organized as follows: First we review a previously reported thruster model. Second, we extend this model to incorporate the effects of rotational fluid velocity and inertia on thruster response. Third, we report a novel method for experimentally determining non-sinusoidal lift/drag curves. The models are evaluated by comparing experimental data with numerical model simulations. The data indicates that thruster models incorporating both enhancements provide superior accuracy in both transient and steady-state response.

*Grosenbaugh is with the Deep Submergence Lab at Woods Hole Oceanographic Institution, Woods Hole, MA, 02543, USA, email: mgrosenbaugh@whoi.edu. Whitcomb is with the Department of Mechanical Engineering, Johns Hopkins University, Baltimore, Maryland, 21218, USA, email: llw@jhu.edu.

Name	Unit	Description
$i_m(t)$	A	Motor Current
$\vec{V}(t)$	$\frac{m}{s}$	Flow Velocity Vector
$v_z(t)$	$\frac{m}{s}$	Axial Flow Velocity
$\omega_\theta(t)$	$\frac{rad}{s}$	Rotational Flow Vel.
$\omega_{\theta_u}(t)$	$\frac{rad}{s}$	Rotational Flow Vel. Upstream
$\omega_{\theta_d}(t)$	$\frac{rad}{s}$	Rotational Flow Vel. Downstream
$p(t)$	$\frac{N}{m^2}$	Pressure
$\Omega_{prop}(t)$	$\frac{rad}{s}$	Prop. Rotational Vel.
$L(t)$	N	Lift Force
$D(t)$	N	Drag Force
$\vec{F}(t)$	Nm^3	Volumetric Body Force Vector
$\bar{F}(t)$	N	Hydrodynamic Force
$\bar{Q}(t)$	Nm	Hydrodynamic Torque
$T(t)$	N	Thrust
$Q_m(t)$	Nm	Torque
$\beta(t)$	rad	Angle of Attack
$\alpha(t)$	rad	Angle of Incidence

Table 1: Nomenclature

2 Experimental Setup

The data were obtained with a newly constructed test facility capable of high bandwidth measurement of 6-DOF thruster forces and torques, propeller position, and 3-DOF fluid velocity[1]. The forces and torques were all measured and logged at $1000Hz$. The force and torque data was low-pass filtered with 5^{th} order zero-phase acausal filter with cutoff frequency of 25Hz to suppress artifacts of the test stand's $50Hz$ fundamental vibration mode. All data (except force and torque) are presented unfiltered.

3 Thruster Dynamics With Axial and Rotational Flow Model

This section first reviews a previously reported finite dimensional thruster model which considers only axial fluid flow [8], then presents a more general model which includes the effects of both rotational and axial flow. Both models are based on the assumption of inviscid and incompressible flow with no velocity component in the radial direction. Using the continuity equation (1) and the standard Euler equations (2) [15, 13], we have

$$\nabla \vec{V} = 0 \tag{1}$$

$$\frac{\partial \vec{V}}{\partial t} + (\vec{V} \bullet \nabla)\vec{V} = -\frac{1}{\varrho}\nabla p + \frac{1}{\varrho}\vec{F}. \tag{2}$$

The terms of (1) and (2) are defined in Table 1. In the equations we have omitted explicit time dependence of variables as defined in Table 1.
We model the propeller as an infinitely thin disc in the the center of the ducted thruster that applies a force and a torque to the fluid flow.

$$\vec{F} = 0 \cdot \vec{e}_r + \frac{1}{0.7R} A_0 \cdot \bar{Q} \cdot \delta(z) \cdot \vec{e}_\theta + A_0 \cdot \bar{F} \cdot \delta(z) \cdot \vec{e}_z \tag{3}$$

The reference frame, Figure 3, is in cylindrical coordinates, and $\delta(z)$ denotes the standard dirac impulse function. Using (3), (2) can be simplified to the following three equations in integral form:

$$\vec{e}_r : \qquad 0 = 0$$

[1]For a detailed description of this test facility the reader is referred to [4] and *http://robotics.me.jhu.edu.*

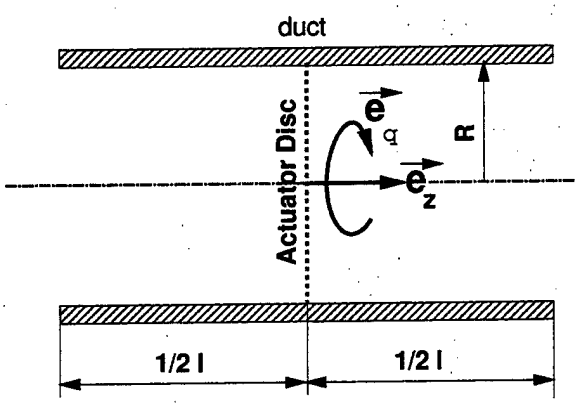

Figure 1: Diagram of coordinate frame and placement of the disc actuator in the duct.

$$\vec{e}_\theta: \quad 0 = -\frac{2}{0.7R}\bar{Q} + \frac{2}{3}\varrho A_0 R \frac{\partial}{\partial t}\int_{-\frac{l}{2}}^{\frac{l}{2}} \omega_\theta dz$$
$$-\frac{2}{3}\varrho A_0 R(\omega_{\theta_u} - \omega_{\theta_d})v_z$$

$$\vec{e}_z: \quad A_0(p_u - p_d) = -\bar{F} + \varrho A_0 l \frac{\partial v_z}{\partial t} \tag{4}$$

Then applying the steady Bernoulli equation and linear momentum theory [18, 8, 16] to large control volumes up and downstream the duct, (4) can be rewritten as

$$\frac{\partial v_z}{\partial t} = \frac{1}{\varrho A_0 l}\bar{F} - \frac{1}{2l} \cdot |v_z| \cdot v_z. \tag{5}$$

3.1 Motor Model

Our Thrusters employ a direct drive DC-Brushless Motor driven by a pulse width modulated (PWM) power amplifier operating in current control mode. The motor mechanical dynamics can be modeled as

$$I_{mech}\,\dot{\Omega} = k_t \cdot i_m - Q_{load} - \text{friction}(\Omega_{prop}) \tag{6}$$

where Q_{load} denotes the motor shaft load.

3.1.1 Experimental Determination of Motor Parameters

The motor has four parameters I_{mech}, k_t, k_{f1} and k_{f0}. The torque constant k_t was provided by the winding manufacturer. A least-square value for the mechanical inertia of the system, I_{mech}, was computed from in-air experimental data. Careful identification of the plant showed that the friction terms are dominated by linear and static friction. Figure 2 shows steady state propeller velocity versus commanded torque in air with no shaft load applied. Table 2 shows the resulting motor parameter values. In order to avoid numerical problems in the subsequent simulations, static friction is modeled with *atan()* instead of the discontinuous *sgn()*. The following friction model is used without exception throughout the paper:

$$\text{friction}(\Omega_{prop}) = \underbrace{k_{f1} \cdot \Omega_{prop}}_{\text{linear friction}} + \underbrace{k_{f0} \cdot \frac{2}{\pi} atan(20 \cdot \Omega_{prop})}_{\text{static friction}} \tag{7}$$

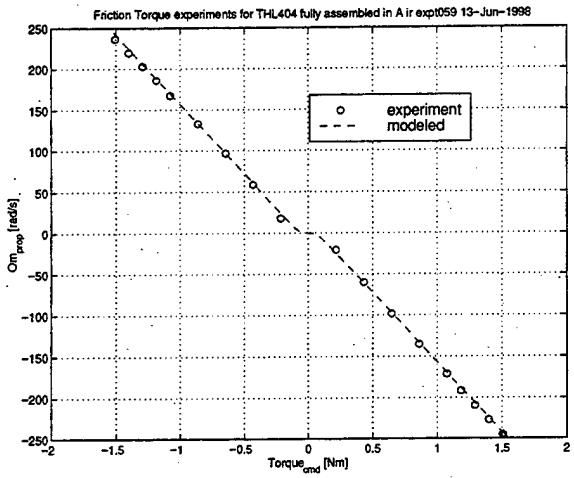

Figure 2: Steady State shaft velocity versus torque in air. Motor friction is dominated by linear and stick friction

3.2 Propeller Model

The following lift and drag functions, [8], are derived from thin airfoil theory:

$$\begin{aligned} L &= 1/2 \cdot \varrho \cdot A_0 \cdot |\vec{V}|^2 \cdot f_L(\beta) \\ D &= 1/2 \cdot \varrho \cdot A_0 \cdot |\vec{V}|^2 \cdot f_D(\beta) \end{aligned} \tag{8}$$

The direction of lift and drag is perpendicular and parallel, respectively, to the direction of the incident flow. Both are related to axial force and motor torque load through a scaled rotation matrix.

$$\begin{bmatrix} \bar{F} \\ \bar{Q} \end{bmatrix} = \begin{pmatrix} 1 & 0 \\ 0 & 0.7R \end{pmatrix} \cdot \begin{pmatrix} -\sin\alpha & -\cos\alpha \\ \cos\alpha & -\sin\alpha \end{pmatrix} \begin{bmatrix} L \\ D \end{bmatrix} \tag{9}$$

3.3 Axial Flow Model

In [8] the authors propose a single term Fourier approximation for lift and drag functions considering only axial fluid flow

$$\begin{aligned} f_L(\beta) &= C_{Lmax} \cdot sin(2\beta) \\ f_D(\beta) &= C_{Dmax} \cdot (1 - cos(2\beta)) \end{aligned} \tag{10}$$

where the angle of attack β is computed as

$$\begin{aligned} \alpha &= atan2(-0.7R\,\Omega_{prop}, v_z) \\ \beta &= \Phi - \alpha - \tfrac{\pi}{2}. \end{aligned} \tag{11}$$

From (5) the axial fluid velocity varies as

$$\dot{v}_z = \frac{1}{\varrho A_0 l}\bar{F} - \frac{1}{2l} \cdot |v_z| \cdot v_z. \tag{12}$$

To experimentally identify parameters for this model we ran combined bi-directional step tests in which the torque command to the motor controller was instantly reversed. The analytical model, (6), predicts that when $i_m = 0$ and $Q_{load} = 0$ then Ω_{prop} will converge to zero in finite time, with the rate of convergence determined by the parameter l. This anticipated effect is clearly observed in the actual experiments, for example in Figure 3 at $t = 11s$. Figure 3 shows the propeller rotational velocity of a $2.15Nm$ torque step and its reversal. The figure compares simulations with different axial flow length values to experimental results. For $l = 0.12m$ the zero velocity time for simulation and experiment match.

Model Independent Parameters			
Parameter	Value	Description	How Obtained
l	$0.12m$	duct length, axial flow length	experiment
l_{w1}	$0.12m$	outer rotational flow length	simulation
l_{w2}	$0.24m$	inner rotational flow length	simulation
l_w	$0.30m$	rotational flow length	simulation
R	$0.123m$	propeller radius	measured
A_0	$0.0475m^2$	duct cross section area	measured
Φ	$0.51rad$	pitch angle	measured
ϱ	$1000\frac{Kg}{m^3}$	density	property
k_t	$0.5392\frac{Nm}{A}$	motor torque constant	manufacturer
k_{f_1}	$0.005913\frac{Nm\ s}{rad}$	linear friction coefficient	experiment least squares fit
k_{f_0}	$0.07278Nm$	stick friction	least squares fit
I_{mech}	$0.0014804\frac{Kg\ m^2}{rad}$	motor,shaft and prop. inertia	experiment least squares fit
Model Dependent Parameters			
Axial Flow model			
K_1	0.3536	axial flow form factor	experiment least squares fit
CL_{max}	0.7629	max. Lift coefficient	experiment least squares fit
CD_{max}	0.2523	max. drag coefficient	experiment least squares fit
Rotational Flow model			
K_1	0.3681	axial flow form factor	experiment least squares fit
K_2	1.1415.	rotational flow form factor	experiment least squares fit
CL_{max}	1.1125	max. Lift coefficient	experiment least squares fit
CD_{max}	0.1703	max. drag coefficient	experiment least squares fit

Table 2: Model parameters

3.4 Rotational Flow Model

In order to have a more complete model we propose to include rotational flow. We used a lumped parameter model that separates the rotational flow into multiple solid body rotations. Figure 4 shows the lengths l_{w1} and l_{w2} which are introduced in order to account for differences in axial and rotational added inertias. The flow up and downstream of the control volume is assumed to be dissipative. With the above assumptions we have to consider two cases of flow regimes depending on the direction of the axial flow.
For $v_z \geq 0$:

$$\begin{aligned}
\dot{\omega}_0 &= -\frac{2}{l_{w2}} \cdot K_2 \cdot \omega_0 \cdot v_z \\
\dot{\omega}_1 &= \frac{2}{l_{w1}} \cdot K_2 \cdot (\omega_0 - \omega_1) \cdot v_z \\
\dot{\omega}_2 &= \frac{2}{l_{w1}} \cdot K_2 \cdot (\omega_1 - \omega_2) \cdot v_z + \frac{2}{\frac{1}{3}\varrho A_0 R^2 l_{w1}} \cdot Q \\
\dot{\omega}_3 &= \frac{2}{l_{w2}} \cdot K_2 \cdot (\omega_2 - \omega_3) \cdot v_z
\end{aligned} \tag{13}$$

For $v_z < 0$:

$$\begin{aligned}
\dot{\omega}_0 &= \frac{2}{l_{w2}} \cdot K_2 \cdot (\omega_0 - \omega_1) \cdot v_z \\
\dot{\omega}_1 &= \frac{2}{l_{w1}} \cdot K_2 \cdot (\omega_1 - \omega_2) \cdot v_z + \frac{2}{\frac{1}{3}\varrho A_0 R^2 l_{w1}} \cdot Q \\
\dot{\omega}_2 &= \frac{2}{l_{w1}} \cdot K_2 \cdot (\omega_2 - \omega_3) \cdot v_z \\
\dot{\omega}_3 &= \frac{2}{l_{w2}} \cdot K_2 \cdot \omega_3 \cdot v_z
\end{aligned} \tag{14}$$

The model also introduces a new form factor, K_2, which makes the steady state values of the rotational flow in the simulations match the experiment. The resulting angle of attack β proposed in [10] includes the mean value of the up and downstream rotational flow into the this model.

$$\begin{aligned}
\alpha &= atan2(0.7R\,(\tfrac{1}{2}(\omega_1 - \omega_2) - \Omega_{prop}), v_z) \\
\beta &= \Phi - \alpha - \tfrac{\pi}{2}
\end{aligned} \tag{15}$$

Axial force and torque are computed in the same way as in the axial flow model by replacing (11) by (15).

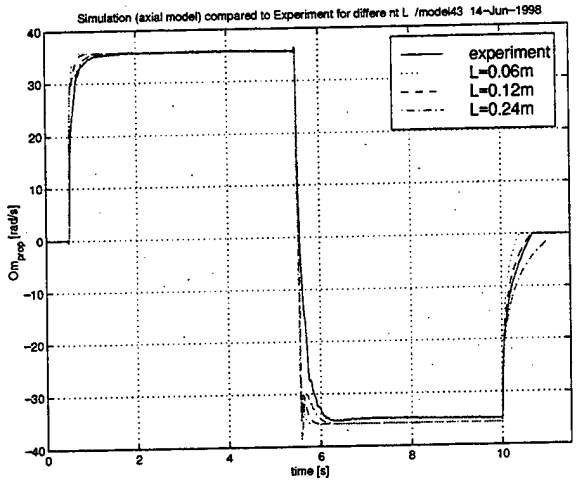

Figure 3: Experimental and simulated Ω_{prop} as a function of time with variation of l in the simulations Torque step of $+2.15Nm$ at $t = 0.5s$, reversing to $-2.15Nm$ at $t = 5.5s$, and to $0.0Nm$ at $t = 10s$.

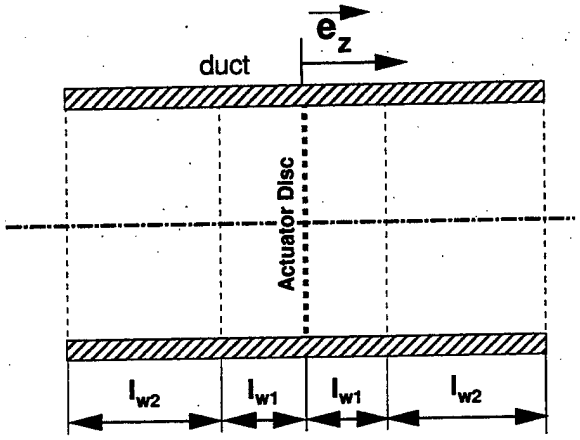

Figure 4: Lump parameters for the rotational flow model.

3.5 Comparison of Axial and Axial plus Rotational Flow Models

Figure 5 shows the results of the model simulations for a $2.15Nm$ torque reversal and actual experimental data. The top plot of Figure 5 shows the axial force versus time. Both models tend to overshoot significantly compared to the experiment; neither model accurately captures the experimentally observed transient response. In particular the expanded rotational model performance is worse than the axial flow model. The bottom plot shows propeller rotational velocities. It also shows considerable discrepancies in the transient behavior between model simulations and actual experiment.

We conclude (*i*) that the additional complexity of the rotational flow model alone does not improve model performance and (*ii*) both models are incapable of accurately reproducing the sharp transient response arising from step torque inputs using experimentally determined parameters. We note that it is possible to "manually tune" a set of parameters which will cause these models to more closely match the transient response of a particular state, e.g. axial force, but this will necessarily cause mis-match in other states, e.g. flow velocities.

4 A New Method for Generating Lift and Drag Curves

Despite the addition of rotational fluid dynamics, the thruster models described in the previous section do not accurately predict actual thruster transient response. This discrepancy motivated us to examine the validity of the

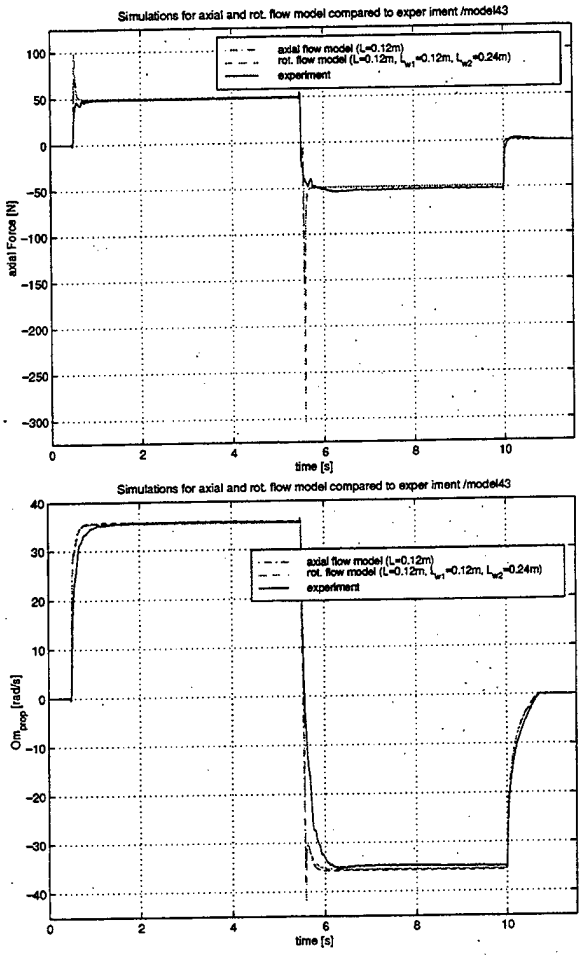

Figure 5: Axial Force versus time (top) and propeller rotational velocity versus time (bottom) simulated using rotational and axial model compared to experimental data. Torque step of $+2.15Nm$ at $t = 0.5s$, reversing to $-2.15Nm$ at $t = 5.5s$, and to $0.0Nm$ at $t = 10s$.

the sinusoidal lift/drag curves, (10), [8, 16], employed in the previous section's models. Previous reports, [8, 16], assumed sinusoidal lift/drag curves, (10), yet were unable to directly verify these curves because their experimental setups did not include precision 3-D fluid velocity instrumentation. We have instrumented our new thruster test facility, [4], to precisely measure the variables (thrust, torque, prop velocity, and 3-D fluid velocity) necessary to experimentally determine lift/drag curves.

4.1 Lift and Drag Curves

Our thruster model assumes lift and drag are functions of the square inflow velocity (8) and dimensionless lift and drag curves. Figure 6 shows the lift and drag coefficients computed from actual experimental data (at three different trust levels), and compares them to the previously assumed sinusoidal lift/drag curves, (10). The figure shows (*i*) a substantial discrepancy between the the experimental lift/drag curves and the sinusoidal lift/drag curves and (*ii*) the experimentally determined lift/drag curves do not vary significantly with torque level.

4.2 Hybrid Simulation

The problem of experimentally generating accurate lift/drag curves is complicated by two problems with real-time measurement of thruster fluid velocity. First is the need to measure fluid flow velocity *at the actuator disk*. With our acoustic doppler flow instrumentation, we were able to measure fluid flow $0.1m$ up and downstream of the thruster's

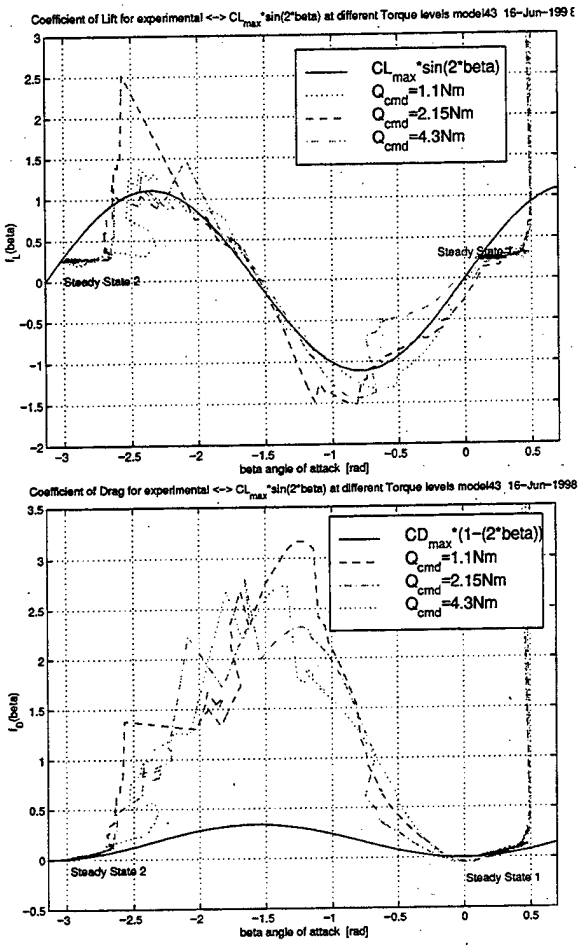

Figure 6: Experimental measured and sinusoidal lift (upper plot) and drag (lower plot) versus angle-of-attack.

propeller. Second, the turbulent flow ejected from the thruster has a high variance in velocity. Both problems limit the accuracy of experimentally determined lift and drag curves.

To address this problem, we have devised a novel "hybrid" technique for generating lift/drag curves utilizing experimental data only for (i) commanded torque, (ii) measured torque, (iii) measured thrust, and (iv) measured propeller rotation velocity. First, these experimentally measured signals are used as the input to a simplified thruster model which estimates fluid velocity as follows:

$$\dot{v}_z = \frac{1}{\varrho A_0 l}\bar{F}_{expt} - \frac{1}{2l}\cdot|v_z|\cdot v_z \tag{16}$$

$$\begin{aligned} I_{mech}\dot{\Omega}_{prop} = \quad & k_t \cdot i_m - Q_{expt} - \\ & k_{f1}\cdot\Omega_{prop} - \tfrac{2}{\pi}atan(20\cdot\Omega_{prop})\cdot k_{f0} \end{aligned} \tag{17}$$

For $v_z > 0$:

$$\begin{aligned} \dot{\omega}_1 &= -\tfrac{2}{l_w}\cdot K_2\cdot\omega_1\cdot v_z \\ \dot{\omega}_2 &= \tfrac{2}{l_w}\cdot K_2\cdot(\omega_1-\omega_2)\cdot v_z + \tfrac{2}{\frac{1}{3}\varrho A_0 R^2 l_w}\cdot Q_{expt} \end{aligned} \tag{18}$$

For $v_z < 0$:

$$\begin{aligned} \dot{\omega}_1 &= \tfrac{2}{l_w}\cdot K_2\cdot(\omega_1-\omega_2)\cdot v_z + \tfrac{2}{\frac{1}{3}\varrho A_0 R^2 l_w}\cdot Q_{expt} \\ \dot{\omega}_2 &= \tfrac{2}{l_w}\cdot K_2\cdot\omega_2\cdot v_z \end{aligned} \tag{19}$$

Second, using the simulated fluid velocity obtained from the "hybrid" simulation and the experimental propeller rotational velocity, we compute the angle of incidence α and angle of attack β as in (15). Third, inverting (9) we compute lift and drag. Finally, the corresponding lift and drag curves can now be computed over a range of angle of attack. Figure 7 shows the generated curves for different torque commands and compares it to the old lift and drag coefficients. The curves represent lift and drag for one torque reversal by using data from the reverse transition we are able to capture the asymmetry of the thruster. These curves serve as a template for new curves shown in Figure 8. These "hybrid" lift and drag coefficients, Figure 8, can be used in the full dynamic thruster simulation as a lookup table.

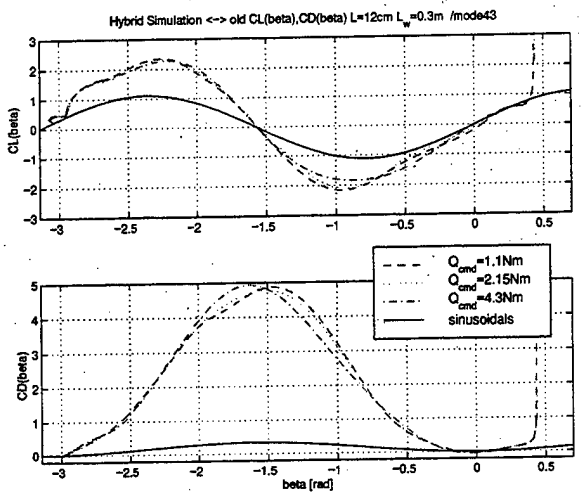

Figure 7: Hybrid and sinusoidal lift and drag coefficients versus angle of attack.

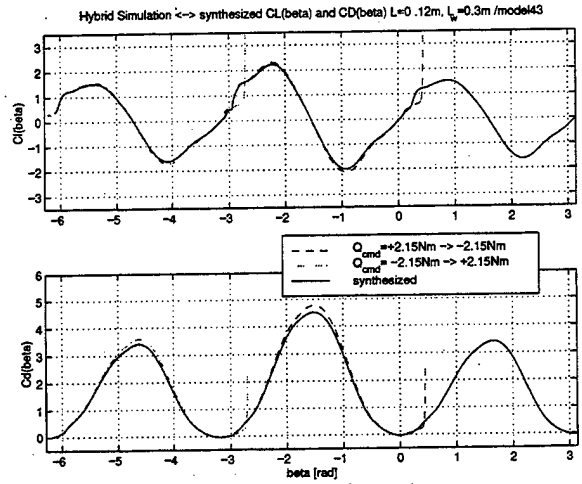

Figure 8: Synthesized lift and drag coefficient versus angle of attack.

4.3 Comparison

Figure 9 shows the results of (a) actual experimental data, (b) a full dynamic thruster model simulation (with rotational+axial flow) using the synthesized lift and drag functions, and (c) corresponding simulations using the sinusoidal lift/drag functions. Figure 9 clearly shows the improvement of the new $f_L(\beta)$ and $f_D(\beta)$ curves. The model using the hybrid lift/drag curves predicts the experimental data with far greater accuracy than the model

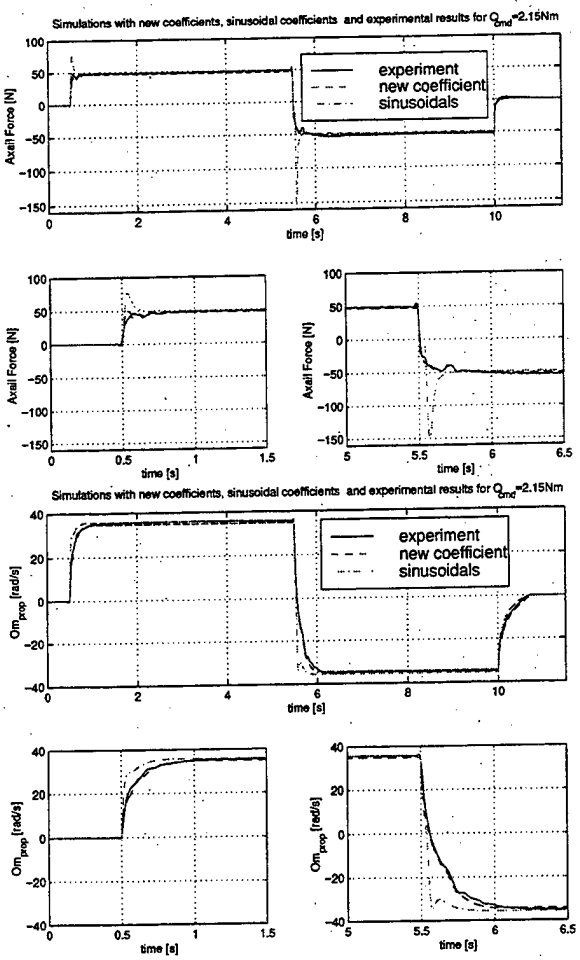

Figure 9: Axial force versus time (top plots) and propeller rotation velocity versus time (bottom plots). Plots show (a) experimental data, (b) model simulation using new lift and drag coefficients, and (c) model simulation using sinusoidal coefficients. Torque step of $+2.15Nm$ at $t = 0.5s$, reversing to $-2.15Nm$ at $t = 5.5s$, and to $0.0Nm$ at $t = 10s$.

employing sinusoidal lift/drag curves. Moreover, the new lift/drag curves also enable the thruster model to capture the forward/reverse asymmetry observed in the thruster experimental data.

Although the hybrid lift/drag curves were computed using experimental data from a single a $2.15Nm$ bi-directional step test, Figure 10 demonstrates that the resulting model is highly accurate for a variety of torque levels.

5 Conclusion and Future Work

We conclude the following:

1. Finite-dimensional thruster models using either axial flow (Section 3.3) or axial+rotational flow (Section 3.4) with sinusoidal lift/drag curves do not accurately reproduce experimentally observed transient response.
2. Experimentally observed lift/drag curves are not simple sinusoids.
3. A novel technique to experimentally determine actual lift/drag curves is reported.
4. Incorporating experimentally derived lift/drag curves into the axial+rotational flow thruster model results in highly accurate correspondence between model and experimental performance for both transient and steady-state operation.

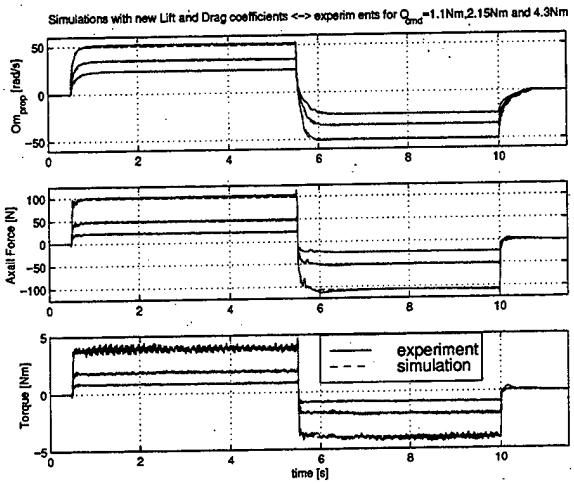

Figure 10: Comparison of experimental data and model simulation using new lift/drag curve for different thrust levels. Propeller rotation velocity (top), Thrust (middle), and Torque (bottom) versus time.

A number of questions remain unresolved. The hybrid modeling approach must be tested and verified with different thrusters and thruster configurations. At present, all model parameters are computed off-line from experimental data – an on-line estimation technique would be useful. Finally, a closed-loop thrust control algorithm incorporating a form of on-line adaptive parameter estimation with a minimum of instrumentation might enable improved model-based thrust control in practical underwater vehicle applications. Such a thrust controller may enable improved closed-loop positioning and tracking for marine vehicles.

Acknowledgement

We gratefully acknowledge the generous help of Dr. Dana Yoerger (WHOI), and the expertise and assistance of Dr. Wade McGillis (WHOI) in acoustic doppler flow measurements.

References

[1] J. Adams, D. Burton, and M. Lee. Dynamic characterization and control of thrusters for underwater vehicles. Techreport, Monterey Bay Aquarium Research Institute and Stanford University Aerospace Robotics Laboratory, September 1991.

[2] B. Allen, R. Stokey, N. Forrester, R. Gouldsborough, M. Purcell, and C. von Alt. Remus: a small, low cost auv; system description, field trials and performance results. In *Proceedings of IEEE/MTS OCEANS'97*, volume 2, pages 994–1000, October 1997.

[3] R. Bachmayer, L. Whitcomb, , and M. Grosenbaugh. A four quadrant finite dimensional thruster model. In *Proceedings Oceans '98*, September 1998.

[4] R. Bachmayer, L. Whitcomb, M. Nakamura, and M. Grosenbaugh. Unsteady three-axis force, torque and flow dynamical modeling and experiments with marine thrusters. In *The 10th International Symposium on Unmanned Untethered Submersible Technology*, October 1997.

[5] R. Bachmayer, L. L. Whitcomb, and M. Grosenbaugh. A four quadrant finite dimensional thruster model. *IEEE Journal of Oceanic Engineering*, 1998 (submitted). (submitted).

[6] N. Brokloff. Matrix algorithm for doppler sonar navigation. In *Proceedings of IEEE/MTS OCEANS'94*, volume 2, pages 378–83, September 1994.

[7] N. Brokloff. Dead reckoning with an adcp and current extrapolation. In *Proceedings of IEEE/MTS OCEANS'97*, volume 2, pages 994–1000, October 1997.

[8] A. J. Healey, S. M. Rock, S. Cody, D. Miles, and J. P. Brown. Toward and improved understanding of thruster dyamics for underwater vehicles. In *Proceedings of the 1994 Symposium on Autonomous Underwater Vehicle Technology*, pages 340–352, Boston, MA, USA, 1994.

[9] J. Knowles, M. Grosenbaugh, and D. Keenan. Numerical simulation of an auv thruster during maneuvering. In *ISOPE-98: Proceedings of the 6th International Offshore and Polar Engineering Conference*, Los Angeles, CA, May 1996.

[10] B. Lakshminarayana. *Fluid Dynamics and Heat Transfer of Turbomachinery.* Wiley-Interscience, New York, USA, 1996.

[11] D. B. Marco and A. J. Healey. Local area navigation using sonar feature extraction and model based predictive control. In *Proceedings of Symposium on Autonomous Underwater Vehicle Technology*, June 1996.

[12] D. Miles, D. Burton, M. Lee, and S. Rock. Closed loop force control of underwater thrusters. Techreport, Monterey Bay Aquarium Research Institute and Stanford University Aerospace Robotics Laboratory, October 1992.

[13] L. M. Milne-Thomson. *Theoretical Hydrodynamics.* Dover Publications, Inc., New York, USA, 1996.

[14] M. Nakamura, R. Bachmayer, L. Whitcomb, and M. Grosenbaugh. H_∞ control of thruster for auv. In *ISOPE-98: Proceedings of the 8th International Offshore and Polar Engineering Conference*, Montreal, Canada, May 1998.

[15] J. Newman. *Marine Hydrodynamics.* MIT Press, Cambridge, Massachusetts USA, 1989.

[16] L. L. Whitcomb and D. R. Yoerger. Comparative experiments in the dynamics and model-based control of marine thrusters. In *Proceedings of IEEE/MTS OCEANS'95*, volume 2, pages 1019–1028, October 1995.

[17] L. L. Whitcomb, D. R. Yoerger, H. Singh, and D. A. Mindell. Towards precision robotic maneuvering, survey, and manipulation in unstructured undersea environments. In Y. Shirai and S. Hirose, editors, *Robotics Research - The Eighth International Symposium.* Springer-Verlag, London, 1998. (In press).

[18] D. R. Yoerger, J. G. Cooke, and J. E. Slotine. The influence of thruster dynamics on underwater vehicle behavior and their incorporation into control system design. *IEEE Journal of Oceanic Engineering*, 15(3):167–178, June 1990.

[19] D. R. Yoerger and D. A. Mindell. Precise navigation and control of an rov at 2200 meters depth. In *Proceedings of Intervention/ROV 92*, San Diego, June 1992. MTS.